Brookhaven National Laboratory
BNL-NUREG-35596 (1984)

Submitted to Acta Metallurgica

A Model for Hydrogen Induced Slow Crack Growth in Hydride Forming Metals

T. M. Ahn
Department of Nuclear Energy
Brookhaven National Laboratory
Upton, New York 11973

Aug-g-no

Submitted to Acta Metallurgica

A Model for Hydrogen Induced Slow Crack Growth in Hydride Forming Metals

T. M. Ahn
Department of Nuclear Energy
Brookhaven National Laboratory
Upton, New York 11973

ABSTRACT

A new model is formulated for the hydrogen-induced slow crack growth kinetics in hydride forming metals. Hydrogen diffusion flux from both stress and concentration gradients is used for the crack growth kinetics at lower temperatures, while hydride nucleation kinetics are evaluated as the crack growth kinetics at higher temperatures. The present formulation explains quantitatively the stress-intensity dependence of the crack growth kinetics, the low activation energies for the crack growth kinetics and the crack jump phenomenon.

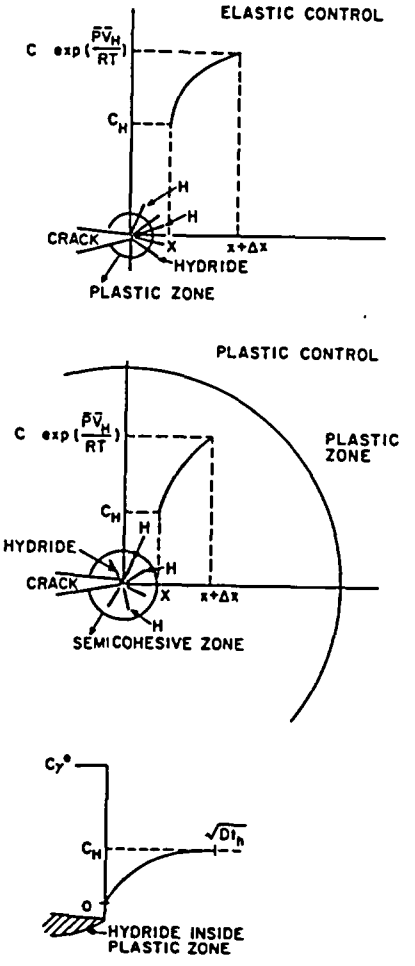

Figure 1. A schematic of hydride growth at a crack tip (a) Stage I, (b) Stage II, (c) hydrogen concentration in front of a growing hydride. C_H is the hydrogen concentration at the interface due to the formation of a concentration profile, x is the hydride or semicohesive zone size, d is the grain size, $C \cdot \exp(\bar{P}\bar{V}_H/RT)$ is the far field hydrogen concentration modified by stress. C_Y^e is the hydrogen concentration in the hydride, $\sqrt{Dt_h}$ is diffusion distance formed in front of a growing hydride, D is the diffusivity, and t_h is the hydride fracture time.

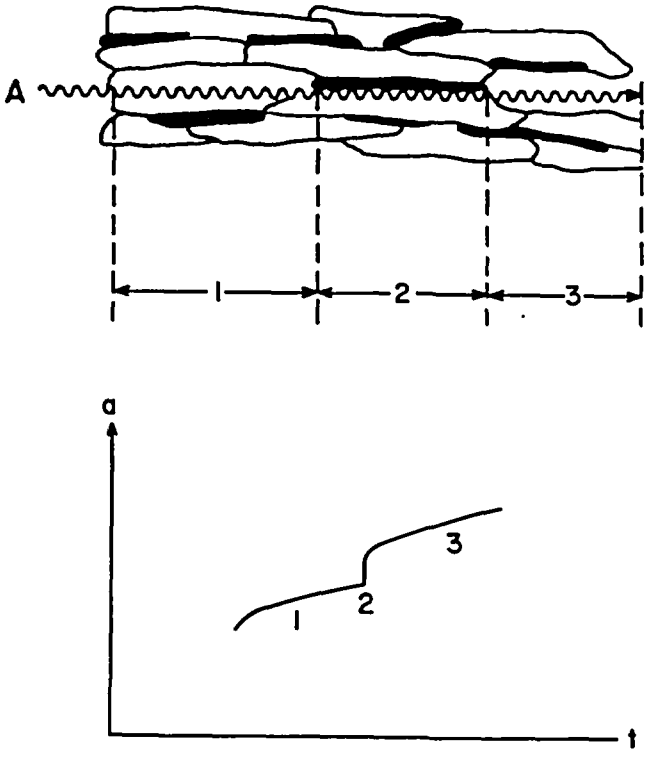

Figure 2. A schematic of crack growth (zigzagged path indicated by A) as the crack front passes through major phase (white grain, 1), interface with minor phase (black grain, 2) and major phase (white grain, 3). The corresponding crack growth kinetics are shown in the lower figure.

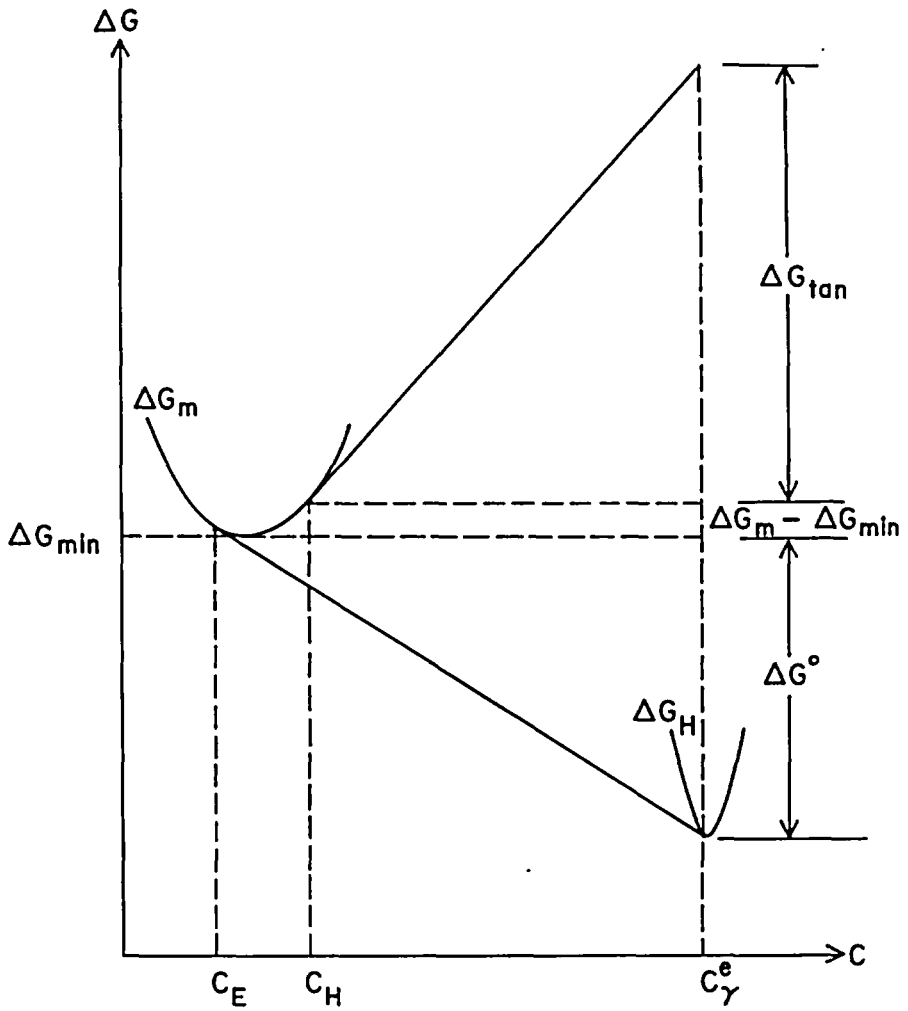

Figure 3. Free energy diagram for major matrix phase (ΔG_m) and hydride phase (ΔG_H). C_E is the hydrogen solubility limit, C^e_γ is the hydrogen concentration in the hydride phase, ΔG° is the free energy change for the hydride formation, ΔG_{min} is the minimum free energy for major matrix phase, and ΔG_{tan} is the tangent of ΔG_m at hydrogen concentration $C = C_H$ times $(C^e_\gamma - C_H)$. The driving force for the hydride nucleation at $C = C_H$ is given by the sum of ΔG_{tan}, $(\Delta G_m - \Delta G_{min})$ and ΔG°[22].

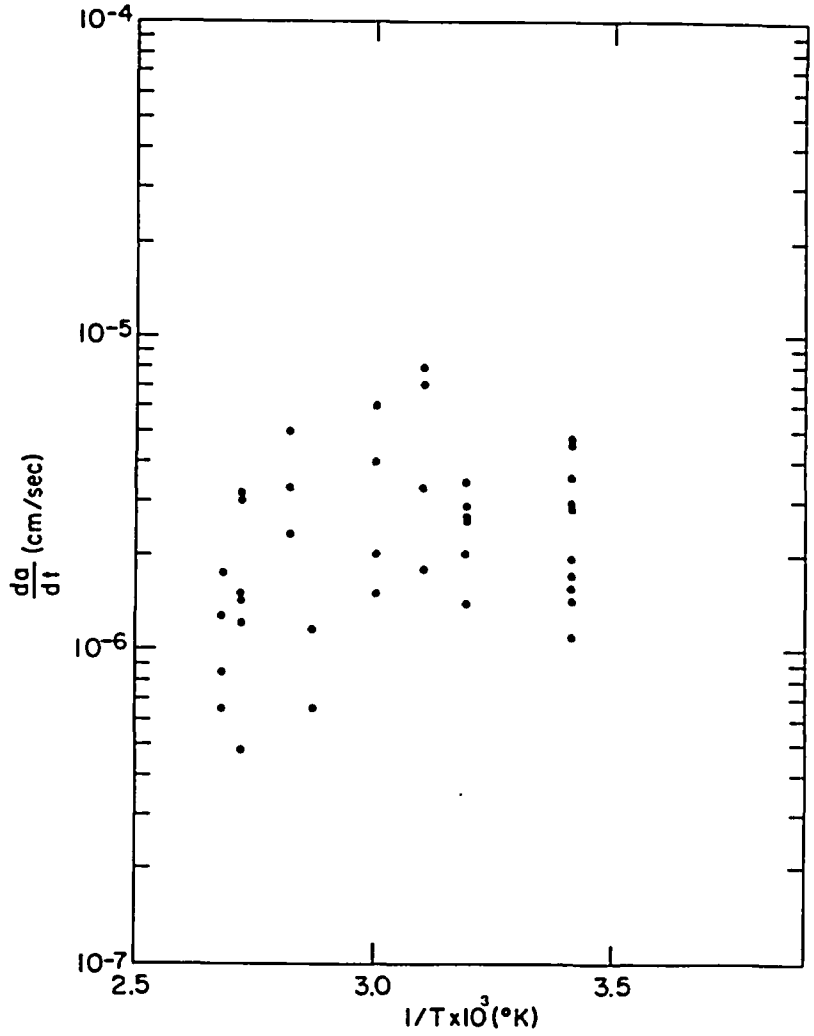

Figure 4. The measured slow crack growth rates for as-received Grade-12 titanium for K = 60 to 80 MPa$\sqrt{m}$ at various temperatures.[16]

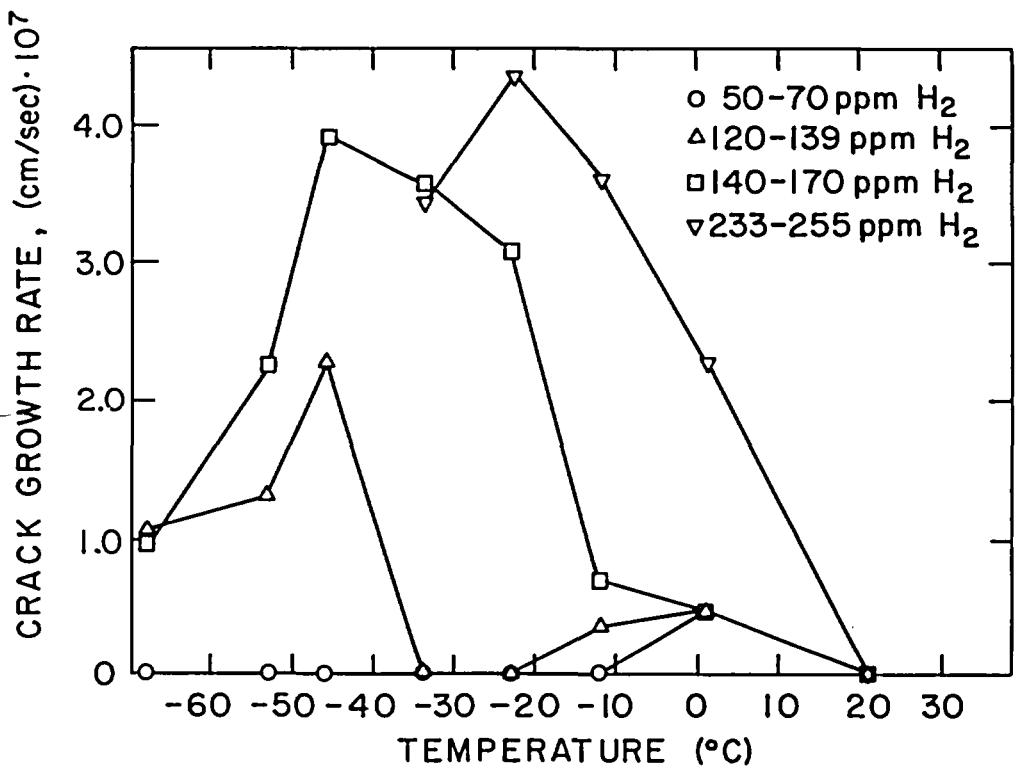

Figure 5. The measured slow crack growth rates of hydrogenated Ti-6Al-4V at various temperatures.[8]

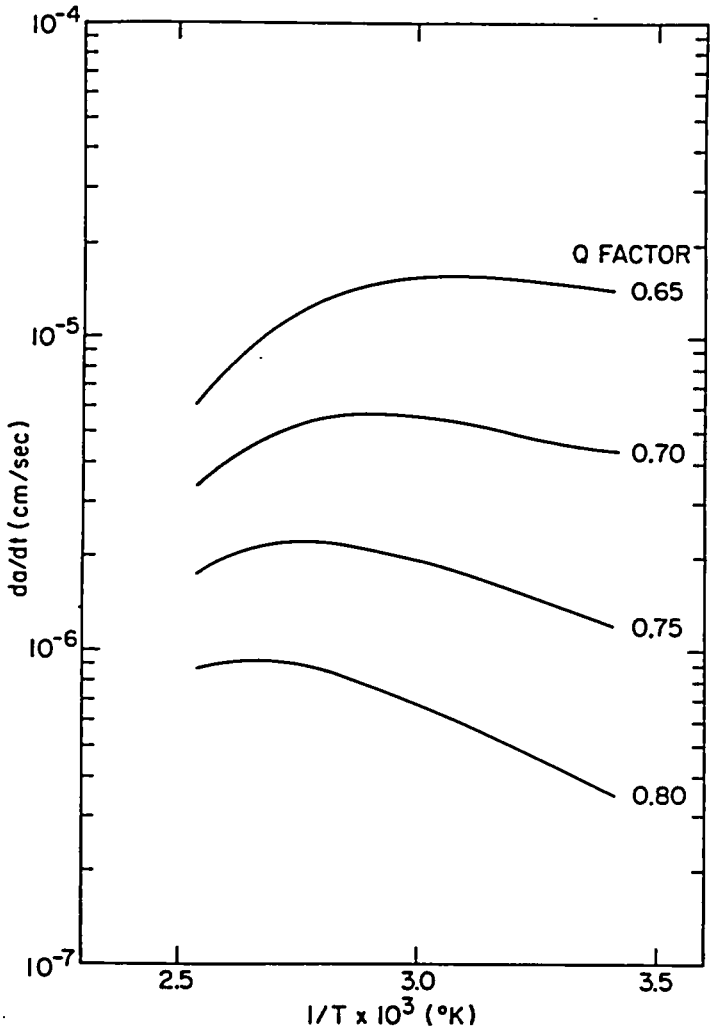

Figure 6. Calculated slow crack growth rates of as-received Grade-12 titanium controlled by hydrogen pipe diffusion for all K values at various temperatures. The Q factor is the ratio of activation energy for pipe diffusion to that for lattice diffusion.

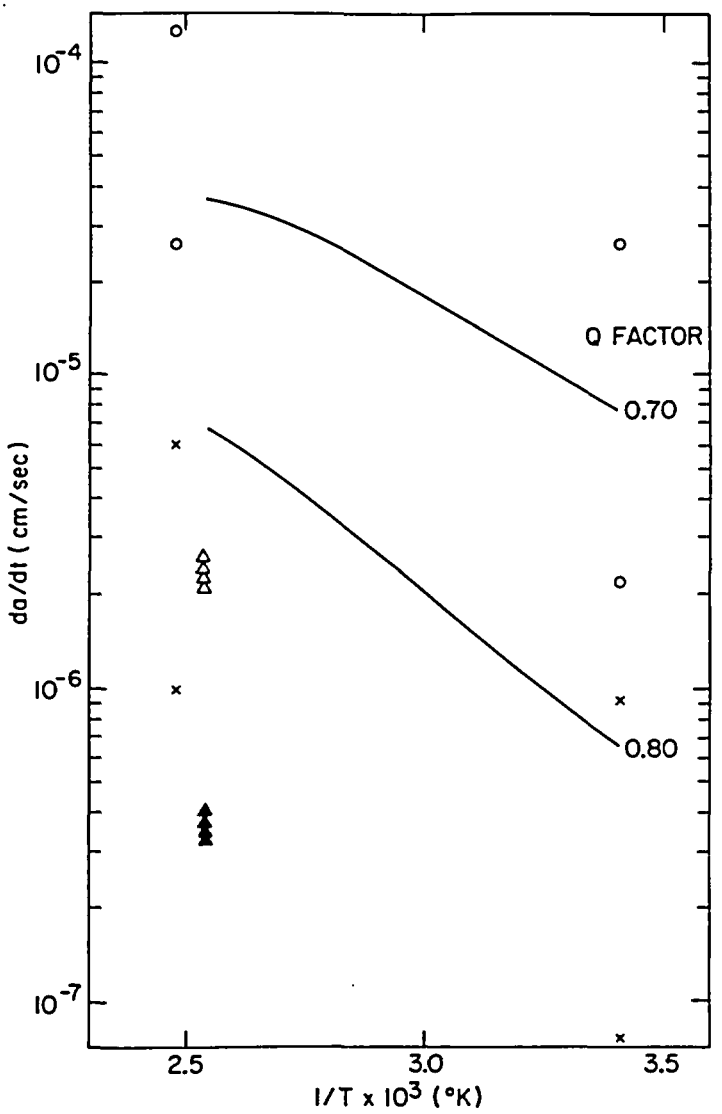

Figure 7. Calculated crack growth rates of as-received Grade-12 titanium assuming hydrogen pipe diffusion kinetics plus nucleation kinetics (triangles). For nucleation control, four triangles are for K = 42, 56, 80, 127 MPa$\sqrt{m}$, respectively from the top in sequence at 120°C. Open triangles are for Q = 0.70 and solid triangles are for Q = 0.80. Open circles are for C_o=50 ppm and x points are for d = 20 μm.

List of Tables

List of Figures

List of Figures (Continued)

Page

1. INTRODUCTION

It is well known that hydride formation is responsible for hydrogen embrittlement in hydride forming metals which include pure metals or alloys of Ti, Zr, Nb, V, or Cb.[1-4] Hydrogen induced slow crack growth kinetics of these materials have been understood on the basis of long range hydrogen diffusion rates from a major bulk matrix, such as the alpha phase in the alpha major - beta minor alloys, to crack tip in most cases. However, the measured activation energies for slow crack growth kinetics are usually lower than for hydrogen diffusion in the major phase matrix[2,5-8] (typically alpha-phase matrix). Also, the crack velocity is often found to decrease at higher temperatures.[6-8]

Table 1 summarizes the relevant data from the literature for the temperature dependence of crack velocity in hydride-forming metals. The observed activation energy is usually lower than the 52 kJ/mole needed for alpha-phase matrix diffusion of hydrogen in titanium[9] and the 70 kJ/mole required for alpha-phase matrix diffusion of hydrogen in zirconium.[2] The observed low activation energies have been attributed to short-circuit diffusion, most likely pipe diffusion along dislocations or beta-phase diffusion.[2] Others have proposed[9] that the observed low activation energy is from hydride formation. However, nucleation kinetics for the hydride do not show a simple activation energy. Therefore, the short-circuit diffusion mechanisms is a more plausible explanation for the low activation energy. Table 1 also shows there is a temperature where the crack velocity is a maximum. This is thought to be connected with a hydrogen solubility limit in the alloy and also hydride nucleation kinetics.[7,9,10]

Table 1. Temperature effects on hydrogen induced crack growth in titanium and zirconium alloys.

Materials	Microstructure	Source of Hydrogen	Temperature (°C)	Activation Energy (kJ/mole)	Temperature Dependence of Crack Velocity
Ti-5Al-2.5Sn[5]	α in β matrix	Gas Environment	-70 to 74	22.8	No maximum
Ti-6Al-6V-2Sn[6]	β in α matrix	Internal (38 ppm)	-50 to 60	-12.6 to -14.2 (high temperature) 14.8 to 16.9 (low temperature)	Maximum
Ti-6Al-6V-2Sn[7]	β in α matrix	Internal (38 ppm)	-13 to 47	27.0~32.8 (K_{th}) 42.6 (K_{IIa})	Maximum
Ti-6Al-4V[8]	β in α matrix	Internal (50-255 ppm)	-68 to 20	9.5~86 (low temperature) -10~-23 (high temperature)	Maximum
Zr-22.5Nb[2]	β in α matrix	Internal (10-140 ppm)	21 to 315	27.5 for 10 ppm 29.7 for 10 ppm 39.9 for 140 ppm 42.2 for 130 ppm 63.5 for 130 ppm	No maximum

Transient crack growth kinetics upon loading or crack growth kinetics with intermittent crack jumps have been previously discussed.[11,12,13] When a crack passes through a second phase or a grain boundary, such jumps are considered to occur because the second phase or grain boundary is usually enriched with hydrogen.[14,15] Both upon loading and upon the crack passage through these phases, high hydrogen concentrations result in a high crack velocity before the equilibrium state at the crack front is achieved.

In the present work, a new model has been developed for hydrogen-induced slow crack growth kinetics incorporating short circuit diffusion and hydride nucleation kinetics. In addition, we also describe the transient crack growth kinetics. The calculated results will be quantitatively compared to our recent data on Grade-12 titanium alloy (Ti-0.3 Mo-0.8 Ni, alpha-beta)[16] and other alloys.[8]

2. MECHANISMS AND ASSUMPTIONS

It is known that a small plastic enclave exists at the tip of a propagating crack, which is a preferential site for hydride nucleation.[9,17] Figure 1 shows a schematic of hydride growth at such a crack tip. In Stage I crack growth where the stress intensity is lower, the plastic enclave is small. Since the hydride size is larger than the plastic enclave, hydride growth and crack propagation upon hydride cracking are controlled by the elastic stress field. For diffusion controlled crack growth, a hydrogen concentration gradient will develop at the crack tip. The far field concentration is a stress enhanced concentration while the concentration at the hydride tip is controlled by a balance between the diffusion flux and the hydrogen consumption rates. The diffusion flux is composed of a concentration gradient term and a stress gradient term. Both are assumed to be rate controlled by second-phase or grain boundary diffusion rates to explain the observed low activation energies for crack propagation rates.

In Stage II crack growth, the plastics enclave is larger than the hydride size and the hydrides are able to reside within a part of this enclave called the semicohesive zone.[7] This is a reasonable explanation for the observed cleavage of some grains at the crack front forming a semicohesive zone composed of cleaved grains separated by ductile ligaments.[18] These hydrides grow as a result of hydrogen migration within the plastic enclave, and crack growth within the semicohesive zone is controlled by plastic stresses. As in Stage I, a concentration gradient will develop at the crack tip. However, unlike Stage I, the diffusion rates in Stage II are assumed to be controlled by

dislocations in the plastic zone, again to explain the observed low activation energies for the crack propagation rates. At the large plastic deformation in the plastic zone, the effects of grain boundaries and second phases are minimal compared to the dislocation effects.

When the diffusion rates are fast compared to hydride nucleation rates, such as the situation at higher temperatures, the hydride nucleation rate is the controlling factor for crack propagation. Hydrides are formed on dislocations by a manner described in a classical nucleation theory.[19,20]

Two types of crack propagation jump have been considered: (1) jumps associated with hydride fracture resulting in striation formation on fracture surface and (2) jumps associated with the passage of the crack front through the alpha-beta interface phase or grain boundary where the hydrogen concentration is enriched by high hydrogen solubility.[14,15] A schematic of such a crack growth mechanism is shown in Figure 2, as the crack front passes through the alpha and beta regions. This type of jump is also observed until the hydrogen concentration profile is formed at crack tip when the initial load is applied, because the initial concentration at the crack tip is greater than the concentration at the crack tip during the steady-state crack growth.

Formulations for linear elastic fracture mechanics are used in the calculation for elastic regime. Plane strains are particularly used, since the deepest crack front (at the center of the propagating crack) is always in the plane strain condition.[21] For the plastic regime, Hill's[21] slip line fields are used to describe the stress field inside the plastic zone.

3. FORMULATIONS

Consider the hydrogen flux to position x in Figure 1. This is give by

$$J_D = D \left\{ \frac{C \exp\left(\frac{\overline{P}\,\overline{V}_H}{RT}\right) - C_H}{d/2} + \frac{C_H\,\overline{V}_H}{RT}\,\frac{\overline{dP}}{dx} \right\} \qquad (1)$$

where D is the hydrogen diffusivity, C exp $(\overline{P}\,\overline{V}_H/RT)$ is the far field hydrogen concentration, C, modified by stress field, $\overline{P}\,\overline{V}_H$, C_H is the hydrogen concentration at the interface due to the formation of a concentration profile, V_H is the partial molar volume of hydrogen in the major phase, d is the grain size, $\overline{p}$ is the averaged hydrostatic pressure over a grain, $\frac{\overline{dP}}{dx}$ is the averaged hydrostatic pressure gradient over a grain, and R and T have their usual meaning. The first term in parenthesis is the concentation gradient in a stress field and the second term is the stress-induced drift velocity. In the far field concentration, C is the hydrogen concentration in the major matrix phase for Stage I, while C for Stage II represents the hydrogen concentration along dislocations which contribute to the growth of numerous hydrides in the semicohesive zone. The C value for Stage II, therefore, can be estimated by

$$C = C_o\, L^D \pi\, b^2 \exp\,(E_B/RT) \qquad (2)$$

where C_o is the hydrogen concentration in the major matrix phase, L^D is the dislocation density in the plastic zone, b is the Burger's vector, $\pi.b^2$ is an approximate value of dislocation core area, and E_B is the binding energy of hydrogen in the dislocation core. The diffusivity D represents the minor phase or grain boundary diffusivity for Stage I while it is the dislocation pipe diffusivity for Stage II. The gradient develops in a distance between the hydrided zone boundary and the nearest grain boundary expressed by Δx in

Figure 1. The Δx values can be zero to one full grain size and it can not exceed one grain length because of the existence of high hydrogen concentration in the grain boundaries as hydrogen sources.[14,15] On average, one half grain size is used for this reason in Equation 1.

The pressure P is given by[21]:

$$\begin{aligned} P &= \frac{2(1+\nu)K}{3(2\pi x)^{1/2}} && \text{for elastic control} \\ P &= \sigma_y \{\ell n\ (1 + x/\rho) + 1/2\} && \text{for plastic control} \end{aligned} \qquad (3)$$

where K is the stress intensity factor, ν is Poisson's ratio, σ_y is the yield strength, and ρ is the crack tip radius.[17] As explained before, the P and dp/dx terms are statistically averaged from x to x+d in Figure 1 since the concentation gradient develops only within one grain. Therefore,

$$\left.\begin{aligned} \overline{p} &= \int_{\ell}^{\ell+d} p\,dx \;/\; \int_{\ell}^{\ell+d} dx \\ &= \frac{4(1+\nu)K}{3.(2\pi)^{1/2}.d} \cdot [(\ell+d)^{1/2} - \ell^{1/2}] && \text{for elastic control} \\ \overline{p} &= \int_{d}^{2d} p\,dx \;/\; \int_{d}^{2d} dx \\ &= \frac{\rho.\sigma_y}{d} \cdot [(1+2d/\rho)\ \ell n\ (1+2d/\rho\ (1+d/\rho)\ \ell n\ (1+d/\rho) - 0.5\ d/\rho] \\ & && \text{for plastic control} \end{aligned}\right\} \qquad (4)$$

$$\overline{\frac{dp}{dx}} = \int_{\ell}^{\ell+d} \left(\frac{dp}{dx}\right) dx \;/\; \int_{\ell}^{\ell+d} dx$$

$$= \frac{2(1+\nu)K}{3.(2\pi)^{1/2}.d} \cdot \left[\ell^{-\frac{1}{2}} - (\ell+d)^{-\frac{1}{2}} \right] \quad \text{for elastic control}$$

$$\left.\begin{aligned} \overline{\frac{dp}{dx}} &= \int_d^{2d} \left(\frac{dp}{dx}\right) dx \;/\; \int_d^{2d} dx \\ &= \frac{\sigma_y}{d} \left[\ell n(1+2d/\rho) - \ell n\,(1+d/\rho) + 1/2\right] \quad \text{for plastic control} \end{aligned}\right\} \quad (5)$$

where ℓ is the average hydride size before fracture. We have assumed one grain size as the semicohesive zone size[18] and the crack tip radius ρ is estimated by[17] $K^2/(\sigma_y E_y)$ where E_y is Young's modulus.

The hydrogen flux of Equation (1) is balanced by the total flux, J_N, to all hydrides by:

$$\begin{aligned} J_N &= \frac{1}{2} \frac{D}{(Dt_h)^{1/2}} L^D \pi b^2 C_H \exp(E_B/kT) \quad \text{for elastic control} \\ J_N &= \frac{x}{2\ell} \frac{D}{(Dt_h)^{1/2}} L^D \pi b^2 C_H \exp(E_B/kT) \quad \text{for plastic control} \end{aligned} \quad (6)$$

where t_h is the intermittent hydride fracture time, $x/(2\ell)$ is an approximate value of the number of hydrides, $(Dt_h)^{1/2}$ is the diffusion distance and $L^D \pi b^2 C_H \exp(E_B/kT)$ is the total concentration of hydrogen in dislocations, which contribute to the growth of many hydrides residing in the semicohesive zone. Two expressions for (6) are identical except that $x=\ell$ is used for elastic control, since hydrides nucleate initially in the plastic zone even for elastic control. Equating (1) and (6) will give an unknown quantity C_H. Once C_H is known, the crack velocity is calculated.

Consider the hydrogen concentration in front of a growing hydride shown in Figure 1C where the moving boundary velocity V is described by

$$V = \frac{D}{\sqrt{Dt_h}} \quad \frac{C_H}{C_\gamma^e}$$

where C_γ^e is the mole fraction of hydrogen in the hydride phase. V is again related to the crack growth velocity $\frac{da}{dt}$ by

$$\frac{da}{dt} = \frac{x}{\ell} V \tag{8}$$

considering the total number of hydrides contributing to crack growth kinetics. The Equation (8) is also written in terms of flux by

$$\frac{da}{dt} = \frac{4}{C_\gamma^e} J_N = \frac{4}{C_\gamma^e} J_D \tag{9}$$

In this case, J_N and J_D are terms using C_H values obtained by equating (1) and (6). Evaluation of (8) and (9) gives the crack growth rates by

$$\frac{da}{dt} = \frac{2}{C_\gamma^e} \quad \frac{k_1}{1 - k_2/f} \tag{10}$$

$$C_H = \frac{k_1}{(f-k_2)} \tag{11}$$

where

$$k_1 = \frac{2 \cdot D \cdot C_o}{d} \quad \exp\left(\frac{\overline{P}\,\overline{V}_H}{R \cdot T}\right)$$

for elastic control

$$k_2 = \frac{D\overline{V}_H}{R \cdot T} \quad \frac{\overline{dP}}{dx} - \frac{2 \cdot D}{d}$$

$$k_1 = \frac{2\pi D C_o L^D b^2}{d} \exp\left(\frac{E_B}{kT}\right) \exp\left(\frac{\overline{P}\cdot\overline{V}_H}{RT}\right) \qquad \text{for plastic control}$$

$$k_2 = \frac{D\overline{V}_H}{RT} \frac{\overline{dP}}{dx} - \frac{2\cdot D}{d}$$

and $$f = \frac{\pi}{2} \left(\frac{D}{t_h}\right)^{1/2} L^D b^2 \exp\left(\frac{E_B}{kT}\right) \qquad \text{for elastic control}$$

$$f = \frac{\pi d}{2\ell} \left(\frac{D}{t_h}\right)^{1/2} L^D b^2 \exp\left(\frac{E_B}{kT}\right) \qquad \text{for plastic control}$$

For the transient crack growth period, the following mass balance is used.

$$J_N \cdot \text{area} = -\frac{dC_H}{dt} \cdot \text{volume} + J_D \cdot \text{area} \qquad (12)$$

where (volume/area) $\simeq x/2$ for the hydride forming zone. Solving the partial differential equation with $C_H = C_H^i$ equal to the initial hydrogen concentration, one obtains the transient crack growth velocity at time t:

$$\left(\frac{da}{dt}\right)_{tr} = \frac{2f}{C_\gamma^e} \left\{\frac{k_1}{(f-k_2)} + \left[C_H^i - \frac{k_1}{(f-k_2)}\right] \exp\left[-\frac{2}{x}(f-k_2)t\right]\right\} \qquad (13)$$

C_H^i is C for the initial loading while it can vary for the crack jump during the crack growth depending on the further loading condition and the crack position.

The solution (Equation 13) gives the initial velocity, $(da/dt)_I$, of the fast crack growth in region 2 of Figure 2 by letting t=o

$$\left(\frac{da}{dt}\right)_I = \frac{2f}{C_\gamma^e} C_H^i \qquad (14)$$

and the time to linear crack growth is given by

$$t_r = \frac{x}{2(f-k_2)} \qquad (15)$$

Under the conditions where crack growth rates are controlled by hydride nucleation rate, the concentration profile disappears and J_N is given by

$$J_N = I_o \cdot \ell^3 \cdot \frac{x}{2} \cdot C_\gamma^e \qquad (16)$$

Where I_o is the hydride nucleation rate and $\ell^3 \cdot \frac{x}{2} \cdot C_\gamma^e$ is the total number of hydrogen atom in all hydrides. The hydride nucleation rates are expressed from the classical nucleation theory [20,22] by

$$I_o = C_o \cdot \exp\left(\frac{\overline{P}\,\overline{V}_H}{RT}\right) \cdot \pi L^D b^2 \; (kT/h) \cdot \exp(E_B/kT) \cdot \exp(-\Delta G^*/kT) \; \exp(-\Delta G_d/RT) \qquad (17)$$

where ΔG^* is the activation energy for hydride nucleation on dislocations and ΔG_d is the activation energy for dislocaion pipe diffusion of hydrogen, h is the Planck constant, and (kT/h) is the frequency factor. ΔG^* is expressed by a classical nucleation theory[20,22] as

$$\Delta G^* = \alpha \; 16 \; \pi \; \sigma^3/(3 \; \Delta G_v^{\,2}) \qquad (18)$$

Where ΔG_V is the driving force for hydride nucleation on a dislocation, σ is the interfacial energy for the hydride-matrix interface and α is the ratio of the hydride nucleation barrier in dislocation to that in the bulk matrix.[20] Following the classical nucleation theory,[22,23] ΔG_V is evaluated as follows.

Figure 3 is a schematic of free energy diagram for the formation of hydride. The free energy ΔG is a function of the hydrogen concentration C. ΔG_m is the free energy for the solid solution of major matrix phase and expressed in terms of the hydrogen concentration C by[24]

$$\Delta G_m = RT \left[(1-c) \; \ell n \; (1-c) + c \; \ell n(\gamma^\circ c) \right] \qquad (19)$$

where γ° is the activity coefficient, which can be approximated by[24]

$$\gamma^\circ = \frac{1}{C_E} \exp\left[\frac{(1-C_E)\ (-\Delta G^\circ)}{(C_\gamma^e - C_E)\ RT}\right] \tag{20}$$

where C_E is the solubility limit of the hydrogen in major matrix phase as shown in Figure 3 and ΔG° is the free energy change upon hydride formation.[25] In this equation (20), it is assumed that major matrix phase is a restricted solid solution, so Henry's law is followed by the solute and Raoult's law by the solvent. The details for Equations (19) and (20) are given in Reference 24. The solubility limit C_E for hydride forming metals are given by[26]

$$C_E = \exp\left[(-\Delta G^\circ + \overline{p}\ \overline{V}_H + Wc - Wp - E_{kk}\ \overline{V}_h\ \overline{P})/RT\right] \tag{21}$$

where $\overline{V}_h$ is the partial molar volume of the hydrogen in hydride, Wc is the total molar strain energy due to constraint during hydride formation, Wp is the plastic work done during hydride formation by dislocation movement, E_{kk} is the stress free transformation strain. The details for Equation (21) are given in Reference 26.

ΔG_H is the free energy for the hydride phase, ΔG_{min} is the minimum free energy for the major phase. Then, the driving force ΔG_V for a hydrogen concentration C_H is the sum of ΔG°, ΔG_m(at $C=C_H$),$-\Delta G_{min}$ and ΔG_{tan}[22] where ΔG_{tan} is the tangent of ΔG_m at $C=C_H$ times $(C_\gamma^e - C_H)$. The details for the driving force for the nucleation in binary alloys are given in Reference 22.

The hydrogen concentration at crack tip, C_H, is expressed by

$$C_H = C_o \exp(E_B/RT) \exp(P\ V_H/RT) \tag{22}$$

C_H is illustrated in Figure 1. Dislocation density is not incorporated for this case since the hydrogen concentration on a single dislocation line is considered for the hydride nucleation. The concentration gradient is no longer present for nucleation controlled kinetics and exp (E_B/RT) term is added since the dislocations enhance the hydrogen concentration on dislocations.

Using the above expression ΔG_V is expressed by

$$\Delta G_V = -[C_H \bar{V}_H + (1-C_H)\, \bar{V}_{Ti}]^{-1} \cdot [\Delta G_{tan} + \Delta G_m - \Delta G_{min} + \Delta G^\circ] \quad (23)$$

and

$$\Delta G_{tan} = RT\, (C_\gamma^e - C_H)\, [\ell n\, C_H - \ell n\, (1-C_H) + \ell n \gamma^\circ] \quad (24)$$

$$\Delta G_{min} = 1/(1 + \gamma^\circ) \quad (25)$$

where $\bar{V}_{Ti}$ is the partial molar volume of the major phase element (Ti for Ti-based alloys) obtained from $\bar{V}_H$.[27] $[C_H \bar{V}_H + (1-C_H)\, \bar{V}_{Ti}]$ in Equation (23) is the conversion factor from energy/mole to energy/volume.

4. CALCULATIONS AND COMPARISON TO EXPERIMENTAL RESULTS

First we shall discuss the functional dependence of the derived equations. Then we compare the calculated results with the experimental values quantitatively. For Stage I, the crack velocity is strongly dependent on the stress-intensity factor because of the exponential dependence of hydrogen concentration on stress as shown in Equations (4) and (10). On the other hand for Stage II, the crack velocity is mildly dependent on the stress-intensity factor because the plastic stress is a strong function of yield strength, which is again shown in Equations (4) and (10). These two types of stress dependence are observed typically in crack-velocity versus stress-intensity curves.[2] Higher hydrogen concentration and smaller grain size increase the diffusion-limited kinetics in Equation (10), which has been predicted before.[2,28] This is also found to be true for the effects of hydrogen concentration and grain size on nucleation-controlled kinetics as shown in Equations (9) and (16). Transient crack growth rates of Equation 13 are initially much faster, then they reach a steady state value, as expected from experimental results,[11-13]. The activation energies for diffusion-limited crack growth kinetics in Equation (10) are much lower than the activation energy for hydrogen diffusion in the major matrix phase. In k_1 of Equation (10), besides the activation energy term involved in the diffusivity D, there are two additional activation energy terms which are positive values to lower the overall activation energy, namely, E_B and $\overline{P}\,\overline{V}_H$. Further, the activation energy for D is typically smaller than the activation energy for the hydrogen diffusion in the major matrix phase when hydrogen transports along dislocations and grain boundaries. Among these three terms of activation energy, the stress term ($\overline{P}\,\overline{V}_H$) is a minor contributor to the overall activation energy.

Crack growth rates are decreased when the temperature is increased either from relatively large binding energy for diffusion-limited kinetics or from the contribution of nucleation kinetics. The temperature dependence of nucleation kinetics is very strong because the temperature dependent driving force for nucleation in Equation (18) is exponentially related to the crack growth kinetics of Equations (9) and (16). This implies that the slow crack growth kinetics stop abruptly when the driving force is zero, i.e., when the solubility limit is reached, as observed experimentally.[8] On the other hand, the binding energy term gives a smooth decrease of crack velocity at higher tmeperatures by decreasing the hydrogen concentration along dislocations in Equation (10).

Next, we shall discuss the calculated values more quantitatively in comparison with the experimental values. Table 2 shows the stress dependence of the crack growth rates calculated from various experimental values ($L=10^{11}/cm^2$, E_B = 0.25 eV, Q = 0.7). Q is the ratio of the activation energy for pipe diffusion to that for lattice diffusion[29] assuming that the pre-exponential terms are the same for both cases. The rest of the parameters are defined in the Appendix. As expected, Stage I kinetics are a strong function of stress intensity while Stage II kinetics are nearly independent. With the same conditions for Stage II, transient crack growth rates of Equation (14) are increased by a factor 266 at 20°C and by a factor 3 at 135°C, and the time to steady state of Equation (15) is less than a second. This implies that crack jumps occur very rapidly on loading or when a crack passes through hydrogen-enriched regions such as grain boundaries. Such a fast jump was reported earlier in the literature.[11-13] Also the effective activation energy is reduced from 52 kJ/mole to 17.5 kJ/mole at 20°C and 2.7 kJ/mole at 130°C by the slope calculations. Such a low activation energy is observed, as

shown in Table 1, and in our recent work on Grade-12 titanium.[16] It should be noticed that the calculated low crack growth rates are obtained purely from the contribution of major phase (alpha phase for Grade 12 titanium) crack growth and do not consider crack growth in interfaces or grain boundaries.

Now we consider the temperature dependence of crack growth rates. Again, the parameters used in the calculation are defined in the Appendix. Specifically, the data for Grade-12 titanium (Figure 4) are addressed quantitatively since they do not include interface or grain boundary fracture. On the other hand, the data for Ti-6Al-4V[8] are addressed qualitatively because they include interface or grain boundary fracture (Figure 5). Figure 6 gives the calculated crack growth rates which are controlled by hydrogen pipe diffusion at various temperatures for all K values to be compared with Figures 4 and 5 ($L = 10^9/cm^2$; $E_B = 0.35$ eV; $t_h = 1$ sec; $Q = 0.65$, 0.70, 0.75, and 0.80). Figure 7 also shows the calculated crack growth rates which are controlled by hydrogen pipe diffusion kinetics (the solid line is for $L = 10^{11}/cm^2$, $E_B = 0.25$ eV, $t_h = 1$ sec, $Q = 0.7$ and 0.8). These parameters are slightly different from those for Figure 6 to see the Arrhenius type behavior more clearly. In Figure 7, nucleation kinetics are also evaluated as shown by triangles at 120°C since significant decreases in crack growth rates are present in these temperature regime. Values of $\alpha = 0.8$ and $\sigma = 1040$ erg/cm^2 are used and the solid triangles are for $Q = 0.7$ while the open triangles are for $Q = 0.8$, and from triangles for each Q value are for K = 42, 56, 80, 127 MPa$\sqrt{m}$ from the top in sequence. A smooth curve as in Figure 6 using one set of α and σ values in this temperature regime is not shown for the nucleation kinetics because they are too sensitive to temperature variation (activation energy: 174 kJ/mole for Q=0.7 and 180 kJ/mole for Q=0.8). Temperatures other than 120°C also show similar behavior with the change of

Table 2. Calculated Steady state crack growth rates (cm/sec) at three different stress intensities

	$K(MPa/\sqrt{m})$	42	56	80
130°C:	Stage I	1.8×10^{-6}	1.3×10^{-5}	4.7×10^{-4}
	Stage II	3.8×10^{-5}	3.8×10^{-5}	3.8×10^{-5}
20°C:				
	Stage I	2.2×10^{-8}	3.3×10^{-7}	4.4×10^{-5}
	Stage II	8.0×10^{-6}	8.0×10^{-6}	8.0×10^{-6}

The ratio of activation energy for pipe diffusion (or grain boundary diffusion) to that for bulk diffusion is 0.7, the pre-exponential terms for both diffusion equations are assumed to be the same, the dislocation density is $10^{11}/cm^2$, and the binding energy of hydrogen to a dislocation core is 0.25 eV. The rest of the parameters are defined in the Appendix.

the parameters α and σ. Figure 6 shows a smooth decrease in the crack growth rates at higher temperatures while Figure 7 shows a sharp drop from the solid line to triangles at 120°C which are chosen arbitrarily for comparison. In reality, a combination of the behavior shown in Figure 6 and the triangles in Figure 7 may explain the behavior in Figures 4 and 5. As shown in Figure 7 by open circles, crack growth rates are increased as the hydrogen concentration is increased from 30 to 50 ppm. Also, when the grain size is increased from 2 μm to 20 μm, the crack growth rates are decreased as shown by x points in Figure 7. This is the numerical confirmation of the qualitative comparison described earlier.

5. DISCUSSION

Quite often, the observed Stage II crack growth rates are more strongly dependent on stress intensity than the predictions from this formulation.[7,28] Occasionally such Stage II crack growth rates are called Stage IIa from this reason.[7] Ideally, most crack growth kinetics are in Stage II because the hydride size is very small[19] compared to the plastic zone size and Stage IIa should not be observed. One probable reason for the existence of Stage IIa is that Stage III (plastic tearing process) begins in the Stage II. The other reason for the existence of Stage IIa is probably the assumption made by Hill's slip line estimation of stress in a plastic enclave.[21] Much higher stresses have been reported than Hill's estimation.[17] At the present time, none of these causes are considered in this formulation.

There is ample evidence that $L^D \leq 10^{11}/cm^2$,[31] $0.1 \leq E_B \leq 0.5$ eV[32,33] and that α and Q are known to be less than unit.[20,29] σ=1040 erg/cm^2 is also in the range of the solid-solid interface energies.[32,37] The hydrogen enrichment factor has been studied in detail by Nair and others.[15] According to their works, our estimation is not unreasonable. Hydride fracture time was monitored by the acoustic emission technique in zirconium and was found to be instantaneous.[38] Therefore, the present assumption of hydride fracture time as an adjustable parameter (one second) is not unreasonable. Other parameters for pure titanium or zirconium can equally well be used for dilute alloys since alloying elements are, quite often, enriched in the minor phase and depleted in the major phase.[39] All the above parameters discussed are not available for every alloy. For precise comparison of experimental results to calculated values, these should be determined first in each alloy.

We have calculated a very short transient time to steady state crack growth rates. Experimentally, we have often observed a longer transient time than the present calculated values although the crack jumped immediately in some cases.[11,12,16] The probable reason for the observed longer transient time is the gradual decrease in the hydrogen enrichment factor as the crack propagates to the interior region of the major phase[15] leading to a steady state crack growth rate that is effectively slower than the initial crack jump velocity. The technique to measure this transient behavior is not yet standardized as discussed elsewhere.[16] We will be better prepared for further interpretation of the transient crack velocity when the technique is well established.

We have attempted to evaluate threshold stress-intensity values using the previous formula based on the solubility limit.[26] Since experimental data of the threshold stress intensity are not available for Grade-12 titanium, quantitative evaluations are not presented. However, in these calculations, we have found that the hydride nucleation time becomes infinity at hydrogen solubility limit. Therefore, the solubility limit formulus[26] gives a true threshold value for extended periods. Experimentally, we may observe larger threshold stress intensity than that obtained from the calculation because the hydride nucleation time may be longer than the testing time at a stress intensity greater than the calculated threshold value. Our calculation shows that such measure of stress intensities are very close to the calculated threshold value, which confirms that the measured threshold value will be equivalent to the calculated threshold value.

It is known that repeated monotonic loading gives slower crack growth rates because of crack retardation effects reported before.[40] However, for

the titanium-based alloys, these effects are negligible. For other materials, the retarded crack growth should be taken into account to estimate the overall crack growth rates. We have not considered the possibility of shear tranformation as the hydride growth mode. If there exists such a case, Figure 1c and Equation (7) should be modified. However, the present formulation will not be changed as far as the rate determining step is the diffusion process of Figures 1a and 1b or the hydride nucleation process. This is the usual case since the shear transformation is much faster than the diffusional transformation. To determine the rate determining step for the hydride growth, further experimental works are necessary in the future.

6. CONCLUSIONS

A new model for hydrogen-induced slow crack growth kinetics was presented. Hydrogen diffusion fluxes controlled by stress and concentration gradients were used to derive slow crack growth kinetics at lower temperatures. At higher temperatures, hydride nucleation kinetics were considered to estimate crack growth kinetics. The calculated slow crack growth kinetics explained the observed Stage I crack growth rates, Stage II crack growth rates, low activation energy, and decreased crack growth rates at higher temperatures. Time-dependent diffusion kinetics were used to derive transient crack growth kinetics upon loading as well as upon the passage of the crack through a minor phase or grain boundary. The calculated transient kinetics are higher than those for the steady state. Higher hydrogen concentration and smaller grain size increase the kinetics for the steady state as well as for the transient state. The transient kinetics and the effects of hydrogen concentration and grain size are consistent with the experimental results.

Acknowledgements

This work was supported by the Nuclear Regulatory Commission (NRC) and the program was coordinated by Dr. M. McNeil of the NRC. The author acknowledges Dr. N. R. Moody of Sandia National Laboratories in Livermore for reading the manuscript and many helpful suggestions made by him. Many thanks are extended to Dr. J. K. Lee of Michigan Technological University for his helpful suggestions on nucleation in binary alloys, and to Dr. P. Soo of Brookhaven National Laboratory for his critical review of the manuscript.

APPENDIX

PARAMETERS USED IN THE CALCULATION

Hydride Concentration in Hydride Phase[30]

C_{γ}^{e} = 0.6580

The Average Initial Hydrogen Concentration

C_o = 30 ppm. There is an enrichment factor near the beta phase or grain boundary[14,15] during hydride nucleation 70 ppm was used for that case.

Dislocation Density in Plastic Zone[31]

L = $10^9/cm^2$ (Figure 6), $10^{11}/cm^2$ (Table 2 and Figure 7)

Burger's Vector[32]

b = 0.59 nm

Binding Energy of Hydrogen to Dislocation Core[32,33]

E_B = 0.35 eV (Figure 6), 0.25 eV (Figure 7)

Partial Molar Volume of Hydrogen in Titanium[26]

$\overline{V}_H$ = 1.68 cm^3/mol

Partial Molar Volume of Hydrogen in Hydride[26]

$\overline{V}_h$ = 12.50 cm^3/mol

Grain Size[34]

d = 2μm (for as-received Grade-12 titanium)

Hydride Size[34]

ℓ = 0.67μm (for as-received Grade-12 titanium)

Hydride Fracture Time

t_h = 1 sec (adjustable)

Young's Modulus[35]

E_y = 110.3 MPa

Free Energy of Hydride Formation[25]

ΔG° = 18.6 kJ/mol

The Total Molar Strain Energy due to Constraint during Hydride Formation[26]

W_c = 7.23 kJ/mole

Plastic Work Done during Hydride Formation by Dislocation Movement[26]

W_p = 0.67 kJ/mole

The Stress Free Transformation Strain during Hydride Formation[26]

E_{kk} = 0.24

Yield Strength[35]

σ_y (20°C) = 538 MPa
σ_y (40°C) = 400 MPa
σ_y (60°C) = 386 MPa
σ_y (80°C) = 372 MPa
σ_y (100°C)= 359 MPa
σ_y (130°C)= 334 MPa

Poisson's Ratio[35]

ν = 0.33

Hydrogen Diffusivity[36]

$D = 0.06 \exp(-Q.7200/T)$ $cm^2/secs$

7. REFERENCES

1. N. E. Paton, and J. C. Williams, in Hydrogen in Metals, I. M. Bernstein and A. W. Thompson, Eds., ASM, p. 409, (1974).

2. L. A. Simpson, and M. P. Puls, Met. Trans. 10A, 1093 (1979).

3. D. G. Westlake, Met. Trans. 245, 1969, (1969).

4. S. Koike, and T. Suzuki, Acta Met. 29, 553 (1981).

5. D. P. Williams, and H. G. Nelson, Met Trans. 3, 2107 (1972).

6. R. J. Lederich, S. M. L. Sastry and P. S. Pao, Met. Trans. 13A, 497 (1982).

7. N. R. Moody, and W. W. Gerberich, Met. Trans. 11A, 973 (1980).

8. R. R. Boyer, and W. F. Spurr, Met. Trans. 9A, 23 (1978).

9. W. J. Pardee, and N. E. Paton, Met. Trans. 11A, 139 (1980).

10. S. M. L. Sastry, R. J. Lederich and B. B. Rath, Met. Trans., 12A, 83 (1981).

11. J. D. Landes, and R. P. Wei, International Journal of Fracture, 9, 277 (1973).

12. K. N. Akhurst, and T. J. Baker, Met. Trans., 12A, 1059 (1981).

13. S. D. Antolovich, P. M. Shete and G. R. Chanani, in Fracture Toughness Part II, ASTM STP-514, (1971).

14. D. N. Williams, "Report on Hydrogen in Titanium and Titanium Alloys," TML Report No. 100, May 16, (1958).

15. S. V. Nair, R. R. Jensen and J. K. Tien, Met. Trans., 14A, 385 (1983).

16. T. M. Ahn, and K. S. Lee, to be published.

17. R. Dutton, K. Nuttal, M. P. Puls and L. A. Simpson, Met. Trans., 8A, 1552 (1977).

18. N. R. Moody, and W. W. Gerberich in Mechanical Behavijor of Materials, Vol. 2, edited by K. J. Miller and R. F. Smith, Pergamon Press p. 512, (1979).

19. J. B. Boyd, Trans. of ASM, 62, 77 (1969).

20. J. W. Cahn, Acta Met. 5, 169 (1957).

21. F. Knott, Fundamentals of Fracture Mechanics, John Wiley and Sons, Inc., New York, Chapter 2 (1973).

22. J. Burke, The Kinetics of Phase Transformation, Chapter 5, Pergamon Press (1965).

23. K. C. Russel, Acta Met. 16, 761 (1968).

24. A. W. Swalin, Thermodynamics of Solids, Chapter 9, Wiley-Interscience, (1972).

25. N. E. Paton, B. S. Hickman and D. H. Leslie, Met. Trans. 2, 2791 (1971).

26. N. R. Moody, and W. W. Gerberich, Scripta Met., 15, 709 (1981).

27. J. Darken, and R. Gurray, Physical Chemistry of Metals, McGraw Hill, p. 240, (1953).

28. W. W. Gerberich, Y. T. Chen and C. St. John, Met. Trans., 6A, 1485 (1975).

29. N. A. Gjostein, Diffusion, ASM, Edited by H. I. Aaronson, (1972).

30. Handbook of Chemistry and Physics, CRC Press, 62nd Ed., (1981-1982).

31. R. Casea-Neri, and D. W. Nix, Acta Met., 22, 257 (1974).

32. J. P. Hirth, and J. Lothe, Theory of Dislocation, McGraw Hill, (1963), Chapter 7, Chapter 14, Appendix.

33. A. S. Nowick, and J. J. Burton, Diffusion in Solids-Recent Developments, Academic Press, p. 272, (1975).

34. T. M. Ahn, H. Jain and P. Soo, "Container Assessment-Corrosion Study of HLW Container Materials, July-September 1983," BNL-NUREG-33940, November (1983).

35. Metals Handbook, Ninth Edition, Vol. 3., Properties and Selection: Stainless Steels, Tool Materials and Special-Purpose Metals, ASM, (1980).

36. T. P. Papazoglou and M. T. Hepworth, Met. Trans. 242, 682 (1968).

37. I. Gomez-Ramirez and G. M. Pound, Met. Trans. 4, 1563 (1973).

38. C. E. Coleman and J. F. R. Ambler, "Susceptibility of Zirconium Alloys to Delayed Hydrogen Cracking," AECL 5942, Atomic Energy of Canada Limited (1977).

39. T. M. Ahn, and P. Soo, "Immersion and Surface Studies for the Crevice Corrosion in a Brine Solution," Extended Abstract for the Electrochemical Society Fall Meeting, Washington, D. C. 1983.

40. K. N. Morman, Jr., and R. G. Dubensky, "Predicting Fatigue Crack Retardation Under Single an Intermittent Overloading," in Cracks and Fracture, ASTM-STP 601 (1975).